Available online at www.sciencedirect.com
ScienceDirect
ISPRS Journal of Photogrammetry & Remote Sensing 63 (2008) 223–236
PHOTOGRAMMETRY & REMOTE SENSING
www.elsevier.com/locate/isprsjprs

A comparison of illumination geometry-based methods for topographic correction of QuickBird images of an undulant area

Jindong Wu [a,*], Marvin E. Bauer [a], Dong Wang [b], Steven M. Manson [c]

[a] Department of Forest Resources, University of Minnesota, St. Paul, MN 55108, USA
[b] USDA-ARS Water Management Research Laboratory, Parlier, CA 93648, USA
[c] Department of Geography, University of Minnesota, Minneapolis, MN 55455, USA

Received 7 October 2006; received in revised form 1 August 2007; accepted 4 August 2007
Available online 10 October 2007

Abstract

The high spatial resolution of QuickBird satellite images makes it possible to show spatial variability at fine details. However, the effect of topography-induced illumination variations become more evident, even in moderately sloped areas. Based on a high resolution (1 m) digital elevation model generated with high-frequency real-time kinematic global position system measurements, this study assessed topographic effects on QuickBird images of an undulant area (with a maximum slope of 7.4°) under different illumination and ground conditions. For land surfaces that were characterized by a non-Lambertian reflection, significant bidirectional variations in spectral radiances were found in all bands. The effectiveness of four illumination geometry-based topographic correction methods was evaluated. The results indicated that the empirical correction was the most effective method for all spectral bands in both solar and view directions, while the cosine correction gave the worst results. The *C* correction (in the solar direction) and the Minnaert correction reduced topographic effects, but not as effectively as the empirical correction. For the Lambertian, topographic effects were substantial only in the near infrared band in the solar direction. Bidirectional variations of spectral radiances in other bands and/or view directions were minimal and topographic corrections may not be necessary. None of these methods significantly changed the spatial variability of spectral radiances, although the histogram distributions were greatly modified by the cosine correction and the Minnaert correction.

Keywords: Bidirectional; DEM; High resolution; QuickBird; Topography

1. Introduction

QuickBird, launched on 18 October 2001, currently provides commercially available satellite imagery with the highest spatial resolution: 2.44 m for multispectral and 0.61 m for panchromatic images at nadir (DigitalGlobe, 2002). The QuickBird satellite sensor has three visible bands (0.45–0.52 μm, 0.52–0.60 μm, and 0.63–0.69 μm), one near infrared (NIR) band (0.76–0.90 μm), and one panchromatic band (0.45–0.90 μm). Because of the increased capability for showing spatial variability at fine details, QuickBird data have offered new opportunities for field-scale remote sensing applications (Coops

* Corresponding author. 115 Green Hall, 1530 Cleveland Avenue North, St. Paul, MN 55108, USA. Tel.: +1 612 624 3459; fax: +1 612 625 5212.
E-mail address: jindong@umn.edu (J. Wu).

0924-2716/$ - see front matter © 2007 International Society for Photogrammetry and Remote Sensing, Inc. (ISPRS). Published by Elsevier B.V.

doi:10.1016/j.isprsjprs.2007.08.004

Table 1
Illumination geometries and pixel sizes of QuickBird multispectral images

Date	DOY	Time	θ^s (°)	φ^s (°)	θ^v (°)	φ^v (°)	Pixel size (m)
18 July 2003	199	12:07:39	28.6	141.7	15.5	287.5	2.4
20 August 2004	233	12:09:50	36.1	150.6	6.2	105.2	2.8

DOY refers to day of calendar year; θ^s and φ^s are sun zenith and azimuth angle, respectively; θ^v and φ^v are satellite view and azimuth angle, respectively.

et al., 2006; Wu et al., 2007a,b). However, the successful application of imagery data still depends on further study of new questions associated with the improvement of image resolutions (Sawaya et al., 2003; Wu et al., 2005). One such question relates to the effect of topography-induced illumination variations on image radiometric properties.

Topographic effects refer to variations in observed radiance from an inclined surface as compared to spectroradiometric responses from a horizontal surface as a function of effective incident angle and emergent angle (Holben and Justice, 1980; Justice et al., 1981). It has long been recognized that topography can modify radiance in both solar and view directions, especially when large terrain variations exist (Proy et al., 1989). For relatively flat (e.g., slope <15%) and small (e.g., 1 km × 1 km) areas, topographic microvariations may not be a problem and are often overlooked for satellite sensors with comparatively coarse resolutions, such as the advanced very high resolution radiometer (AVHRR) or the moderate resolution imaging spectrometer (MODIS). Such variations become a concern, however, in the application of QuickBird images even in a very small undulant area due to the high spatial resolution.

Table 2
Results of regression analysis and accuracy assessment of different interpolation methods

Methods	Interpolation (n=7216)			Validation (n=801)		
	Slope	Intercept	RMSE (m)	Slope	Intercept	RMSE (m)
IDW	0.998	0.549	0.043	0.998	0.528	0.045
Ordinary Kriging	0.999	0.231	0.039	1.000	0.080	0.039
Local polynomial	0.993	1.795	0.091			
Global polynomial	0.986	3.772	0.210			

Slope and intercept are parameters of the linear regression between interpolated and measured elevations; RMSE is the corresponding root-mean-square-error.

Changes in topography over short distances could create significant spatial variations in the effective solar incident angle. Additionally, QuickBird images are often acquired at various off-nadir angles to increase the spatial coverage and the temporal frequency of image acquisition. This further complicates topographic effects because effective emergent angles can also change across an image (Barnsley, 1984).

A number of methods have been developed to correct the effect of topographic variation on satellite images. For instance, a mask was developed to partition images into shaded areas and non-shaded areas, and partitioned scenes were processed separately (Baral and Gupta, 1997; Giles, 2001). Band ratioing has frequently been used to reduce the effect of topography by assuming that topography-induced illumination variations are wavelength-independent (Colby, 1991; Crippen, 1988). More rigorous

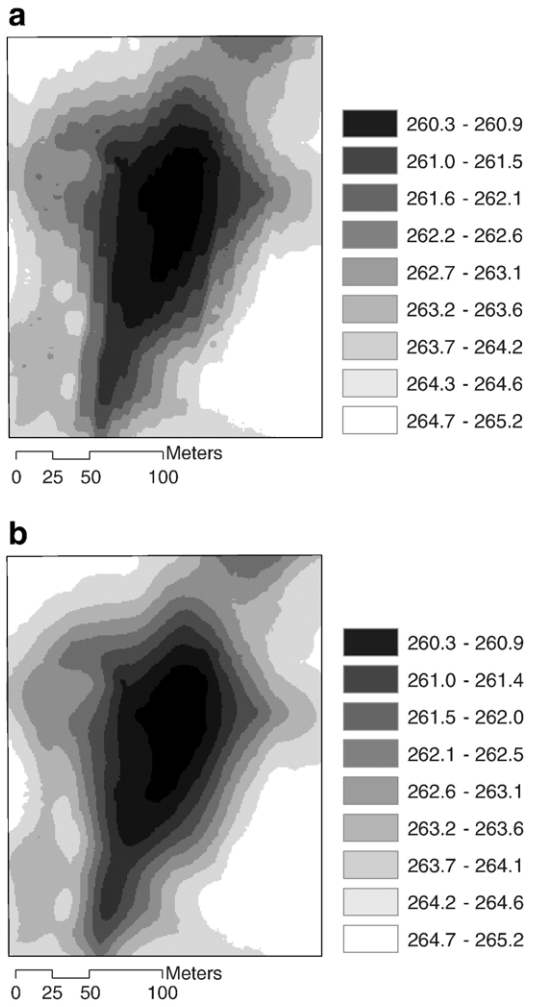

Fig. 1. DEMs generated with the inverse distance weighted (a) and the ordinary Kriging interpolation (b).

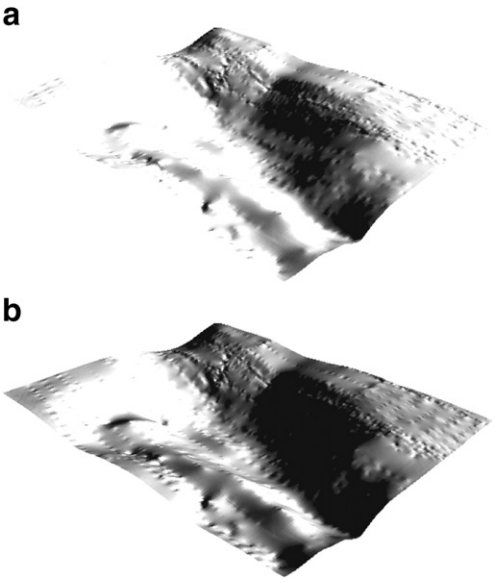

Fig. 2. Hillshaded relief draped over the DEM under the illumination conditions of the 2003 scene (a) and the 2004 scene (b).

methods combine topographic correction with atmospheric correction using radiative transfer models (Conese et al., 1993; Kawata et al., 1988; Richter, 1997; Sandmeier and Itten, 1997; Shepherd and Dymond, 2003).

Illumination geometry-based methods attempt to reduce the complexity of radiative transfer models, but maintain physical coherence (Civco, 1989; Ekstrand, 1996; Smith et al. 1980; Teillet et al., 1982). Landsat Thematic Mapper (TM) data have been used extensively to test the effectiveness of these corrections in the solar direction (Colby and Keating, 1998; Itten and Meyer, 1993; Meyer et al., 1993; Riaño et al., 2003). The empirical, *C*, and Minnaert corrections demonstrated impressive reductions of topographic effects, and the cosine correction was found to have limitations in rugged terrains.

In these methods, the illumination geometry of each pixel is derived with a co-registered digital elevation model (DEM). The effectiveness of topographic corrections often depends on the accuracy and the resolution of the DEMs (Conese et al., 1993). However, the 30 m resolution of currently available DEMs is too coarse to be used for investigating topographic effects in small and moderately sloped areas. A DEM with a resolution finer than QuickBird images should be generated to evaluate topographic effects in these areas. The development of real-time kinematic (RTK) and light detection and ranging (LIDAR) technology has made it possible to collect elevation data with high point density and accuracy. High-frequency collection avoids the inadequacy of data sampling and subsequent errors associated with spatial interpolations. It is possible to produce a DEM for non-flat terrains with absolute elevation accuracy up to 0.15 m by using airborne LIDAR (Huising and Gomes Pereira, 1998). RTK global position system (GPS) measurements provide similar or even better capability (height accuracy ~0.05 m) to capture topographic microvariations and have benefits when applied in agricultural fields (Schmidt and Persson, 2003).

This study had two objectives: 1) to assess the effect of topography-induced illumination microvariations on QuickBird images of crop canopies in an undulant area, and 2) to compare the effectiveness of different illumination geometry-based methods for topographic correction.

2. Methods

2.1. Data collection

The study area (45°23′N, 93°50′W) was located in a moderately sloped agricultural field of about 250 m × 300 m at Becker, Minnesota. GPS measurements were collected with an Ashtech Z-Surveyor, which is a RTK GPS unit with a built-in ultra-high-frequency (UHF) radio and 12-channel all-in-view operations. The horizontal and vertical root-mean-square-error (RMSE) of RTK positions are 1 cm±2 ppm and 1.7 cm±2 ppm, respectively. Elevation data were taken after the crop harvest along 25 tracks in a north–south direction with a 2 s frequency. Random measurements were also taken in a west–east direction to add mass points and to remove potential trend errors. All together, about 10,000 data points were collected. To ensure the quality of measurements, a filter was applied, i.e., position dilution of precision (PDOP) ≤2.3, satellite vehicle (SV) ≥5, and RMSE ≤0.06 m. This process left 8017 data points, in which 6726 data points were within the boundaries of the study area with a density of one point per 10 m^2.

Two QuickBird images were acquired under different ground and illumination conditions in 2003 and 2004 (Table 1). The 2003 image was taken over a fully-closed corn canopy in the middle of the growing season (July 18), while the 2004 image was taken over a partially-closed corn canopy late in the growing season (August 20). In addition, the 2003 image was acquired at a lower solar zenith, but with a higher off-nadir view angle than the 2004 image. The images were also acquired at different azimuth directions; the 2003 image was taken at the forward side, while the 2004 image was taken at the backward side of the incident solar radiation.

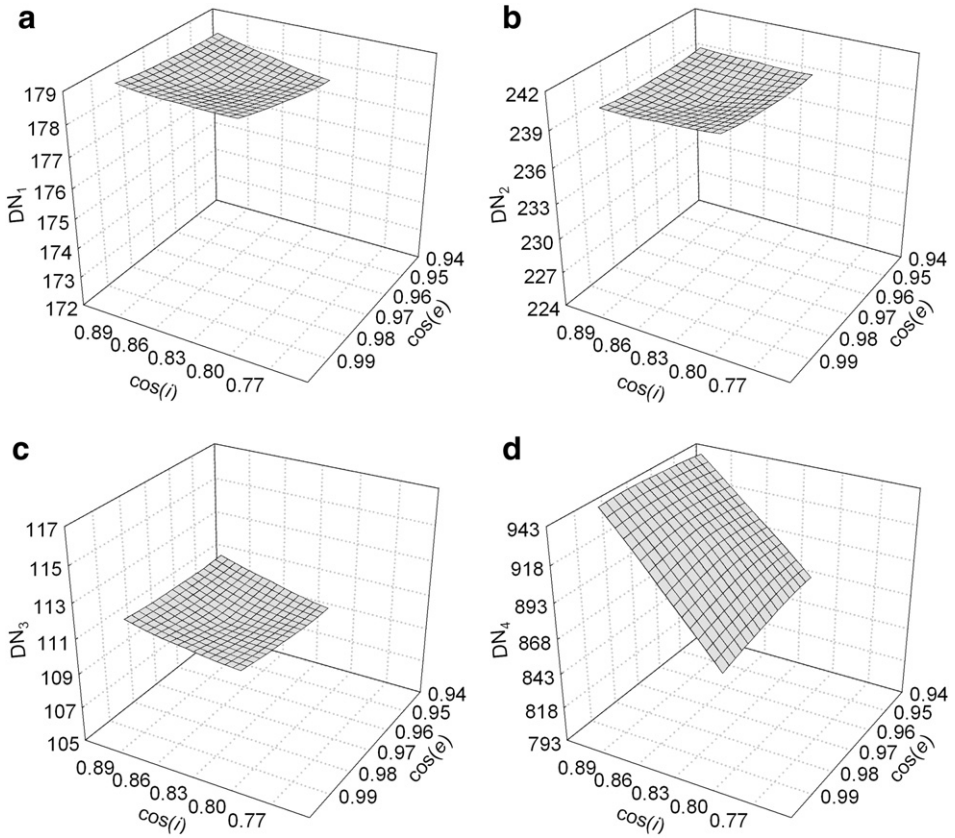

Fig. 3. Dependence of QuickBird spectral radiances (blue (a), green (b), red (c), and near infrared (d)) on solar incident angle (i) and emergent angle (e) with respect to local topography observed on 18 July 2003. DN_1, DN_2, DN_3, and DN_4 are digital numbers corresponding to radiances of the blue, green, red, and near infrared bands, respectively.

2.2. DEM generation and assessment

All 8017 GPS data points were used in spatial interpolations to avoid edge effects. The data were split into two independent sets by the random selection of total GPS data population; 90% of the data (7216 samples) were used in the grid interpolation and DEM generation and 10% of the data (801 samples) were used in the accuracy assessment.

Four different interpolation methods were used to produce grid data with regular 1 m square cells: inverse distance weighted (IDW), ordinary Kriging (no trend was assumed in the data), local polynomial, and global polynomial. A variable search radius was used in the interpolation to search for at least 10 and up to 25 neighbors. The power of the IDW (3.9) and the polynomial interpolations (1.0 for local and 10.0 for global) and the weight of the local polynomial interpolation (4.58) were optimized through geostatistical analyses. A spherical variogram model was used in the ordinary Kriging, and no anisotropic effect was considered. The accuracy of the DEM was assessed by comparing the generated grid values with the reserved data, as described above.

2.3. Correction of topographic effects

Four different topographic correction methods based on illumination geometry were applied to the two QuickBird images: empirical correction, cosine correction, C correction, and Minnaert correction. The solar zenith and azimuth, and the satellite view angle and azimuth were read from the QuickBird Image Metadata (IMD) files. Terrain attributes including slope and aspect were derived from the generated 1 m DEM and resampled to the corresponding QuickBird spatial resolutions with the nearest neighbor method.

2.3.1. Empirical correction

The empirical correction is based on the linear correlation between digital number (DN) or radiance and

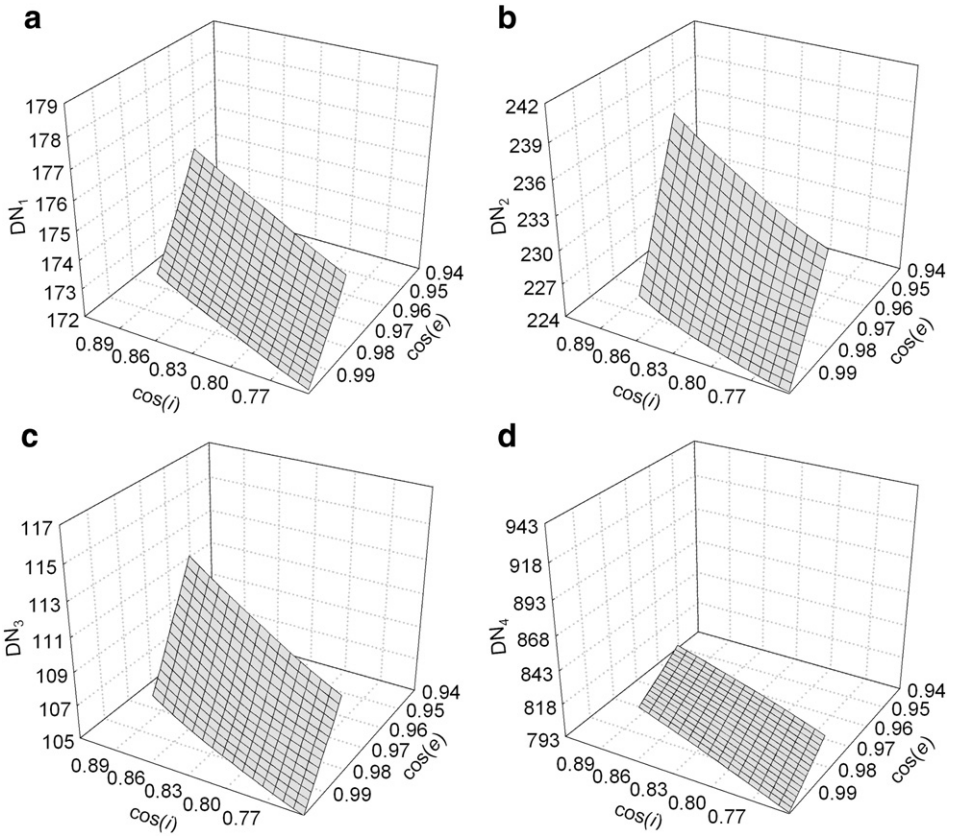

Fig. 4. Dependence of QuickBird spectral radiances (blue (a), green (b), red (c), and near infrared (d)) on solar incident angle (i) and emergent angle (e) with respect to local topography observed on 20 August 2004. DN_1, DN_2, DN_3, and DN_4 are digital numbers corresponding to radiances of the blue, green, red, and near infrared bands, respectively.

illumination geometry (Meyer et al., 1993). Since the QuickBird images were not acquired at nadir, we extended the empirical correlation to both solar and view directions.

$$L_\lambda^{\mathrm{H}}(x,y) = L_\lambda^{\mathrm{T}}(x,y) - \cos\left(i(x,y)\right)m_\lambda^i - \cos\left(e(x,y)\right)m_\lambda^e - b_\lambda^{ie} + \overline{L_\lambda^{\mathrm{T}}} \quad (1)$$

where $L_\lambda^{\mathrm{H}}(x,y)$ is the spectral (λ) radiance that would be observed for horizontal surfaces for an image pixel at column x and row y, $L_\lambda^{\mathrm{T}}(x,y)$ is the corresponding radiance observed over sloped terrain, $\overline{L_\lambda^{\mathrm{T}}}$ is the average of $L_\lambda^{\mathrm{T}}(x,y)$, $i(x, y)$ is the effective incident angle and $e(x, y)$ is the effective emergent angle with respect to the normal of a pixel (x, y). Both $i(x, y)$ and $e(x, y)$ were calculated with the methods proposed by Teillet et al. (1982) based on the sun-satellite geometry (Table 1) and the local slope and aspect for each pixel. The terms m_λ^i and m_λ^e are the regression coefficients and b_λ^{ie} is the constant of the regression between $L_\lambda^{\mathrm{T}}(x,y)$ and both $\cos(i)$ and $\cos(e)$ as the independent variables.

2.3.2. Cosine correction

Under the assumption of Lambertian surfaces, the cosine correction (Holben and Justice, 1980; Teillet et al., 1982) has been extensively used to correct for illumination variations (e.g., Meyer et al., 1993; Riaño et al., 2003).

$$L_\lambda^{\mathrm{H}}(x,y) = L_\lambda^{\mathrm{T}}(x,y)\cos\left(\theta^{\mathrm{s}}\right)/\cos\left(i(x,y)\right) \quad (2)$$

where θ^{s} is the solar zenith angle. As shown in the equation, the cosine correction reduces topographic effects by modifying only the direct part of the incoming irradiance. Diffuse irradiance is not taken into account. The cosine method, therefore, often overly increases the radiance of weakly illuminated areas ($i(x, y)\rightarrow 90°$) where a considerable amount of radiation is diffuse irradiance (Meyer et al., 1993; Teillet et al., 1982). Additionally, no corrections are made in the view direction and this may become a problem for off-nadir viewing sensors like QuickBird.

Table 3
Statistics of the 18 July 2003 QuickBird image before and after topographic corrections

Band	Uncorrected				Empirical correction				Cosine correction				*C* correction				Minnaert correction			
	m_λ^i	m_λ^e	r^2	σ	m_λ^i	m_λ^e	r^2	σ	m_λ^i	m_λ^e	r^2	σ	m_λ^i	m_λ^e	r^2	σ	m_λ^i	m_λ^e	r^2	σ
B	10.0	14.1	0.01[a]	2.6	0.04	−0.04	0[b]	2.6	−194.7	13.0	0.63[a]	4.3	−132.4	13.6	0.44[a]	3.5	−36.9	156.5	0.12[a]	2.8
G	35.3	−17.6	0.01[a]	5.3	−0.05	−0.05	0[b]	5.3	−239.2	−18.3	0.39[a]	6.8	−155.7	−17.7	0.21[a]	6.0	−38.9	164.6	0.04[a]	5.4
R	26.9	8.6	0.02[a]	3.4	−0.04	0	0[b]	3.4	−99.4	8.4	0.20[a]	3.8	−61.0	8.7	0.09[a]	3.6	−20.2	82.5	0.02[a]	3.5
NIR	735.6	−71.4	0.10[a]	39.3	0.04	0.02	0[b]	37.2	−295.6	−89.2	0.02[a]	37.6	18.0	−82.3	0[b]	37.2	−39.7	164.4	0.00[a]	40.7

m_λ^i and m_λ^e are the coefficients of the regression between image digital numbers and the cosine of effective incident angle and effective emergent angle for each band (blue (B), green (G), red (R), and near infrared (NIR)); r^2 is the corresponding coefficient of determination; σ is the standard deviation of image digital numbers across the study area.

[a] Indicates r^2 is significant at $\alpha=0.05$.

[b] Indicates that the correlation is not significant.

2.3.3. C correction

To weaken the cosine correction when $i(x, y)$ approaches 90°, a constant parameter (c_λ) was proposed (Teillet et al., 1982).

$$L_\lambda^H(x,y) = L_\lambda^T(x,y)(\cos(\theta^s) + c_\lambda)/(\cos(i(x,y)) + c_\lambda) \quad (3)$$

$$c_\lambda = m_\lambda / b_\lambda \quad (4)$$

where m_λ and b_λ are the slope and intercept of the regression between $L_\lambda^T(x,y)$ and $\cos(i)$. As Teillet et al. (1982) stated, Eq. (3) could be considered to emulate the effect of diffuse irradiance although the physical analogies are not exact.

2.3.4. Minnaert correction

The Lambertian assumption is not generally valid for vegetated land surfaces (Colby, 1991; Hugli and Frei 1983; Kriebel, 1978). Smith et al. (1980) introduced the Minnaert constant (k), which is a measure of the extent to which a surface is Lambertian (Minnaert, 1941). The value of k changes with spectral band and was derived by linearizing Eq. (5) with a logarithmical transformation.

$$L_\lambda^T(x,y) = L_\lambda^H(x,y)\cos^{k_\lambda - 1}(e(x,y))\cos^{k_\lambda}(i(x,y)) \quad (5)$$

After linearization, k_λ was computed as the slope of the linear regression between $\ln(L_\lambda^T(x,y)\cos(e(x,y)))$ and $\ln(\cos(e(x,y))\cos(i(x,y)))$. The determined k_λ values were then used in the backwards radiance transformation (Eq. (6)) to calculate spectral radiance that would be observed for horizontal surfaces.

$$L_\lambda^H(x,y) = L_\lambda^T(x,y)\cos^{1-k_\lambda}(e(x,y))/\cos^{k_\lambda}(i(x,y)) \quad (6)$$

2.4. Assessment of topographic effects and topographic corrections

Each ground resolution cell corresponding to a pixel in the QuickBird images had unique solar incident and emergent geometry (i.e., $i(x, y)$ and $e(x, y)$). The hillshaded values (i.e., illumination intensity) of each

Table 4
Statistics of the 20 August 2004 QuickBird image before and after topographic corrections

Band	Uncorrected				Empirical correction				Cosine correction				*C* correction				Minnaert correction			
	m_λ^i	m_λ^e	r^2	σ	m_λ^i	m_λ^e	r^2	σ	m_λ^i	m_λ^e	r^2	σ	m_λ^i	m_λ^e	r^2	σ	m_λ^i	m_λ^e	r^2	σ
B	24.5	−144.4	0.02[a]	3.2	−0.03	0.01	0[b]	3.2	−194.0	−146.8	0.63[a]	5.3	10.4	−144.4	0.01[a]	3.2	−1.6	10.2	0[b]	3.3
G	59.1	−534.8	0.03[a]	7.5	0.01	0.05	0[b]	7.4	−229.7	−532.0	0.36[a]	9.3	38.4	−534.3	0.02[a]	7.5	30.8	−331.1	0.01[a]	7.6
R	45.1	−269.8	0.03[a]	4.5	−0.04	0.01	0[b]	4.5	−91.8	−268.7	0.21[a]	5.0	19.2	−269.3	0.02[a]	4.5	17.1	−190.0	0.01[a]	4.7
NIR	327.8	−1343.0	0.03[a]	32.6	0.03	0.01	0[b]	32.1	−705.1	−1373.5	0.21[a]	36.2	97.6	−1347.4	0.01[a]	32.2	63.8	−769.3	0.00[a]	33.8

m_λ^i and m_λ^e are the coefficients of the regression between image digital numbers and the cosine of effective incident angle and effective emergent angle for each band (blue (B), green (G), red (R), and near infrared (NIR)); r^2 is the corresponding coefficient of determination; σ is the standard deviation of image digital numbers across the study area.

[a] Indicates r^2 is significant at $\alpha=0.05$.

[b] Indicates that the correlation is not significant.

cell were computed by considering the local topography and the local illumination angles of both scenes (Table 1) (Burrough and McDonell, 1998). The spectral radiance of each pixel (i.e., $L_\lambda^T(x,y)$) and the corresponding solar incident and emergent geometry were plotted in 3D graphs to illustrate the bidirectional variation of $L_\lambda^T(x,y)$ as a function of $i(x, y)$ and $e(x, y)$. To present the major trend of $L_\lambda^T(x,y)$ variations, the scattered data points were smoothed using the locally weighted scatter plot smooth method (i.e., the LOESS method) with the first degree of local polynomials, a bandwidth of 0.1, and the tri-cube weight function (Cleveland and Devlin, 1988).

The effectiveness of topographic corrections was evaluated with both the statistics (i.e., the correlation of DNs with $i(x, y)$ and $e(x, y)$) and the visual appearance of each spectral band before and after applying the different methods. The more effective the topographic corrections are, the lower the correlation after the corrections. To compare changes in visual appearance of uncorrected and corrected images, each spectral band was draped over the generated DEM to create an orthographic image in a perspective view. This was displayed with the same color map of the uncorrected image. Thus, the same color represented the same value in all images for a specific band; the change of both DN values and spatial variability was comparable. However, for the visible bands, low DNs were presented in a green (or white) color and high DNs were presented in a red (or black) color, while for the NIR band, an inverted color map was used, i.e. low and high DN values were represented in a red (or black) and a green (or white) color, respectively. As a result, for all bands, a dark red (or black) color always represented bare soil and a dark green (or white) color always represented healthy vegetation. The standard deviation of the DNs across the study area and a histogram of the distribution of the imagery data were also computed to assess changes in spatial variability and frequency distribution as a result of different topographic corrections.

3. Results

3.1. Accuracy assessment of interpolations and generated DEM

The IDW and the ordinary Kriging were more accurate for elevation interpolation than the two polynomial methods (Table 2). The RMSE of both the

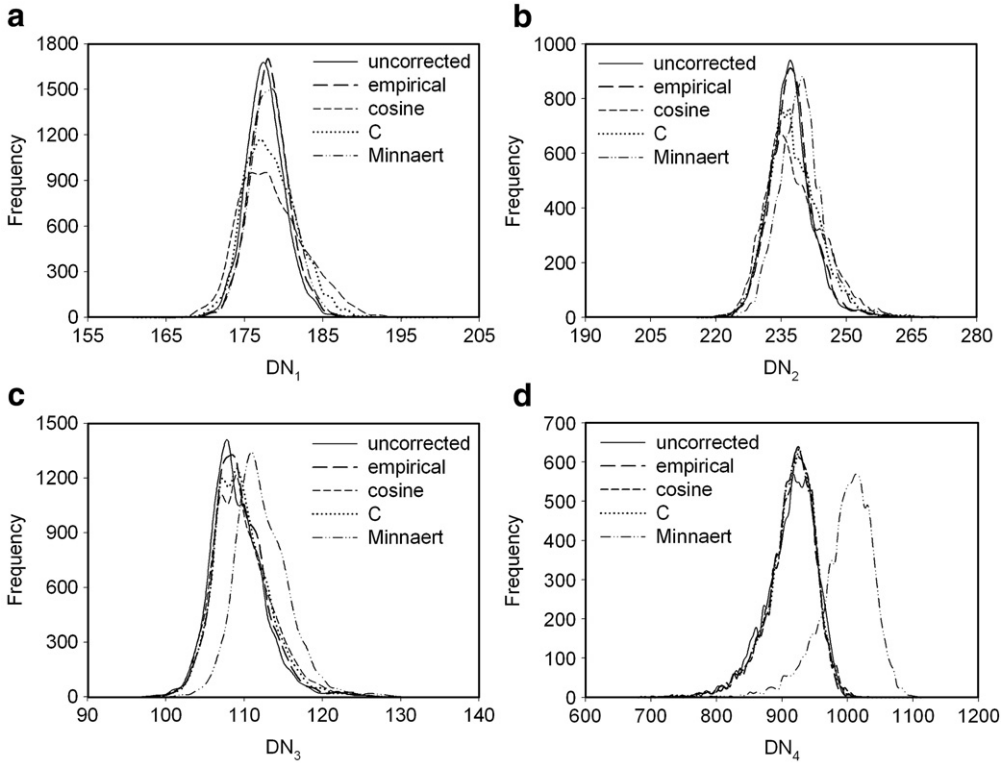

Fig. 5. Histogram distributions of the uncorrected QuickBird image acquired on 18 July 2003 and the topographically corrected images with different methods. DN_1, DN_2, DN_3, and DN_4 are digital numbers corresponding to the blue, green, red, and near infrared bands, respectively.

IDW and the ordinary Kriging was the lowest (~0.04 m) with the highest slopes (~1) and the lowest intercepts (~0) of the regressions between the predicted and the measured elevations. The data points were widely dispersed in the scatter-plots with the polynomial methods (figures are not shown), particularly with the global interpolation (RMSE=0.21 m).

Based on the comparison, the IDW and the ordinary Kriging were selected to interpolate GPS measurements so as to generate a regular grid DEM with 1 m resolution (Fig. 1). By visual comparison, it appeared that the DEMs produced with both methods were almost identical to each other. However, the contour lines of the DEM with the ordinary Kriging changed more smoothly and had fewer abrupt changes than those with the IDW.

Further tests of the generated DEMs against the independent dataset indicated that the two methods had very similar accuracy. The RMSE was 0.045 m and 0.039 m for the IDW and the ordinary Kriging, respectively (Table 2). The slopes of the regression lines with both methods were very similar (~1), although the intercept with the ordinary Kriging (0.08) was lower than that of the IDW (0.53). Based on the visual comparison and the independent accuracy assessment, the DEM generated with the ordinary Kriging had slightly higher accuracy and was chosen as the final DEM to derive slope and aspect for topographic corrections.

The final generated DEM showed that the study area is moderately undulating with a maximum slope of 7.4° or 13% and the surface elevation increasing from 260.3 m to 265.2 m. On the other hand, the study area is oriented towards different directions with the aspect (φ^t) varying from 0° to 360°.

3.2. Bidirectional variations of QuickBird spectral radiances

The hillshaded relief surfaces showed that the 2003 scene had a better illumination condition than the 2004 scene (Fig. 2). However, for both scenes, areas oriented east to southeast (φ^t=67.5°–157.5°) (in a white color) received a relatively high illumination intensity, while areas oriented north to northwest (φ^t=0°–22.5° and 292.5°–360°) (in a black color) were shaded with a relatively low illumination intensity.

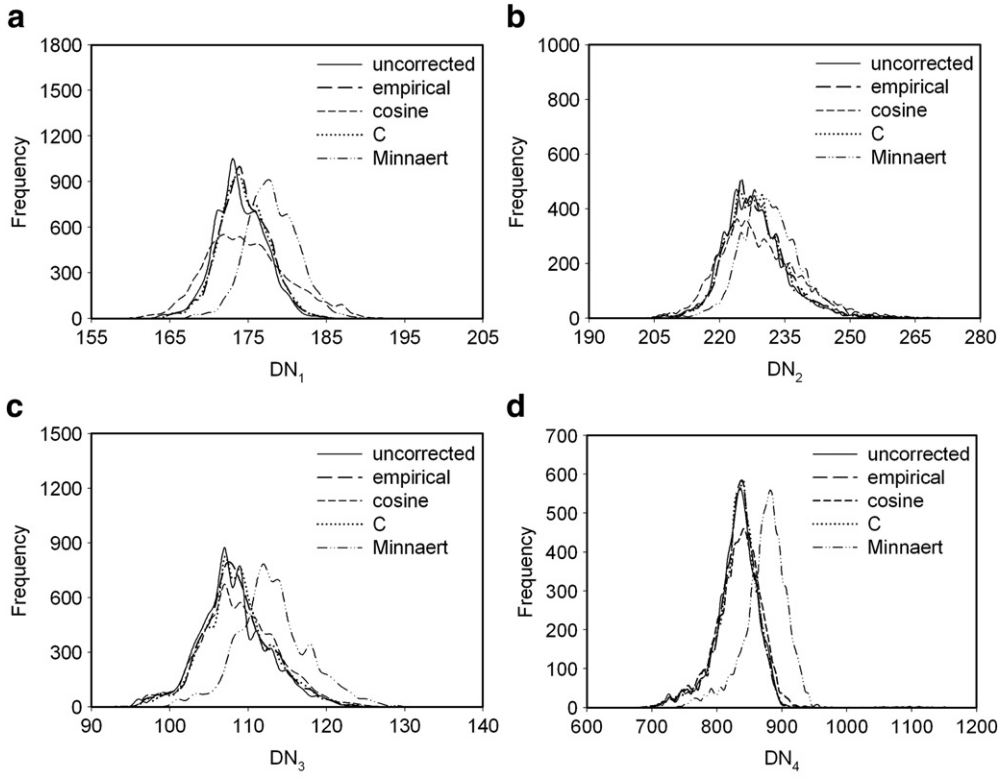

Fig. 6. Histogram distributions of the uncorrected QuickBird image acquired on 20 August 2004 and the topographically corrected images with different methods. DN_1, DN_2, DN_3, and DN_4 are digital numbers corresponding to the blue, green, red, and near infrared bands, respectively.

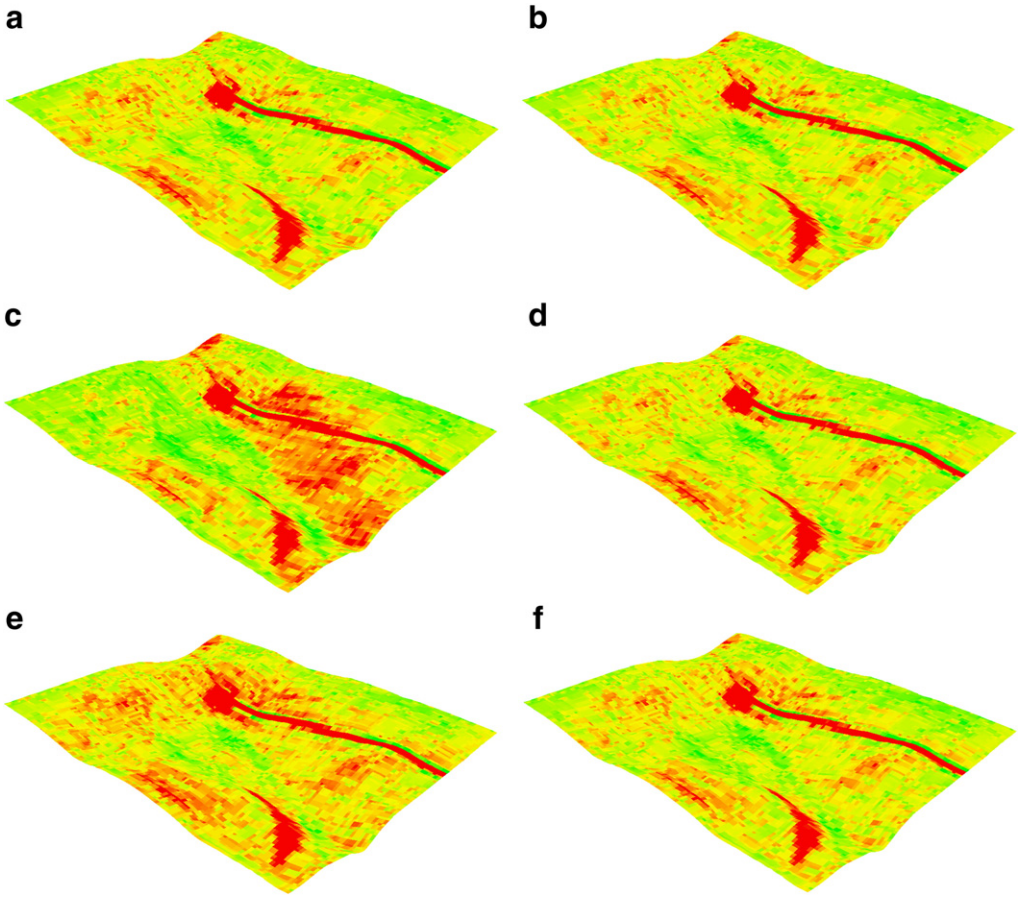

Fig. 7. Uncorrected QuickBird image in green band acquired on 18 July 2003 (a) and topographically corrected images with the empirical correction (b), the cosine correction (c), the *C* correction (d), and the Minnaert correction (e), which is also stretched to its own minimum and maximum values (f). All images are draped over the DEM.

The spectral radiances observed with the QuickBird satellite sensor generally changed in both the solar and view directions (Figs. 3 and 4). However, the magnitude of the variations was different for individual scenes and spectral bands. Compared with the 2004 image (discussed below), the 2003 image was acquired at a lower θ^s (28.6°) (Table 1) and $i(x, y)$ (23.1°–34.9°). The variations of the spectral radiances in the solar direction were minimal for the visible bands, while the spectral radiance in the NIR band increased significantly with a decreasing $i(x, y)$ (i.e., increasing cos(i)) (Fig. 3). Negligible variations of the spectral radiances were found in the view direction, although the satellite sensor had a higher off-nadir viewing ($\theta^v = 15.5°$) and $e(x, y)$ was up to 20°.

The 2004 image was acquired at a higher θ^s (36.1°) (Table 1) and larger $i(x, y)$ (30.7°–42.3°). Radiances in all spectral bands increased with a decreasing $i(x, y)$ (Fig. 4). Large variations of the spectral radiances were also found in the view direction, although the satellite sensor had a nearly nadir viewing ($\theta^v = 6.1°$) and $e(x, y)$ was less than 12°. It was found that the spectral radiances increased with an increasing $e(x, y)$ (i.e., decreasing cos(e)), which indicated that higher spectral radiances were observed when $e(x, y)$ gets close to $i(x, y)$ because of the hot-spot effect.

The regression of DN values with solar (cos(i)) and view (cos(e)) directions showed that the QuickBird spectral radiances of both images were correlated with illumination and observation geometry (Tables 3 and 4). The coefficients of determination were moderate but statistically significant. The absolute values of m_λ^i and m_λ^e of all 2004 image bands were generally higher than those of the 2003 image except the m_λ^i for the NIR band (i.e., m_{NIR}^i). The NIR band of the 2003 image was found to be closely correlated with $i(x, y)$ as shown earlier (Fig. 3d) and the m_{NIR}^i for 2003 was larger than that of the 2004. The absolute m_λ^e values of the 2004 image were in particular much higher than those of the 2003 image.

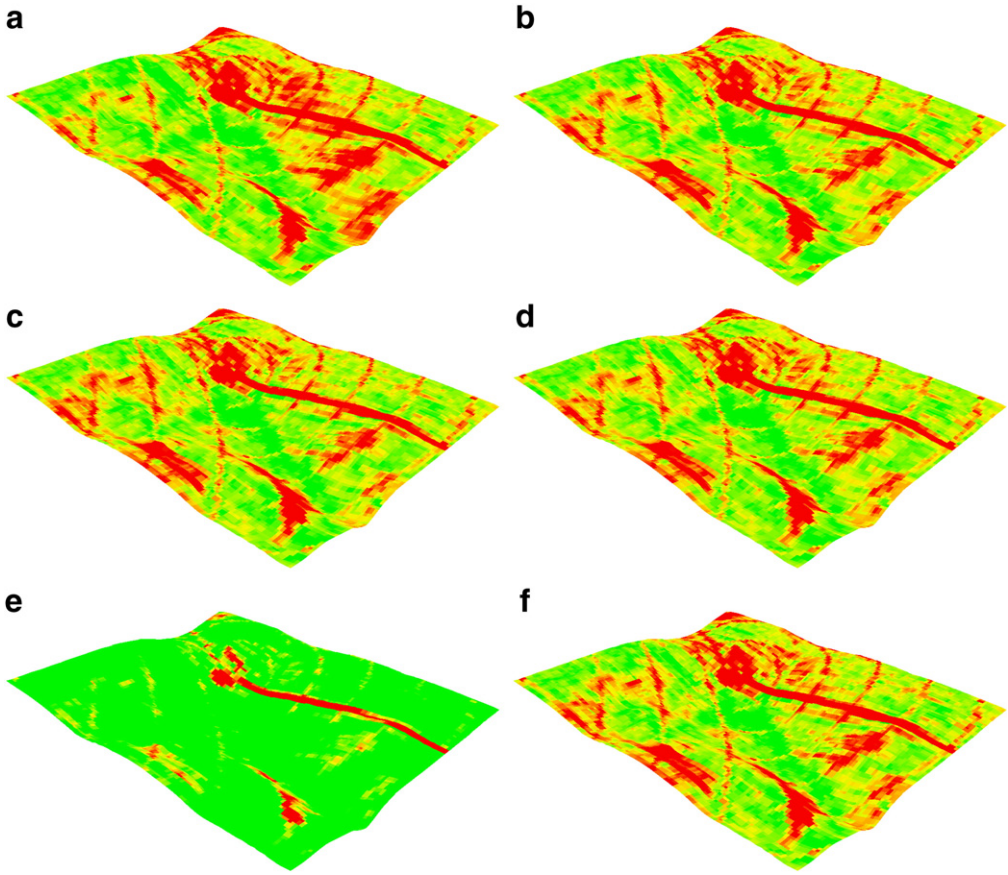

Fig. 8. Uncorrected QuickBird image in near infrared band acquired on 18 July 2003 (a) and topographically corrected images with the empirical correction (b), the cosine correction (c), the *C* correction (d), and the Minnaert correction (e), which is also stretched to its own minimum and maximum values (f). All images are draped over the DEM. Red or black circle lines are the depressed tracks traversed by the sprinkler irrigation system.

3.3. Statistical evaluation and comparison of topographic corrections

The effectiveness of topographic corrections varied with the methods used (Tables 3 and 4). The empirical correction proved to be the most effective method for all spectral bands in both solar and view directions. The empirically corrected DN values of both images were not significantly correlated with $i(x, y)$ and $e(x, y)$ (i.e., $m_\lambda^i \sim 0$, $m_\lambda^e \sim 0$, and $r^2 \sim 0$). The worst performance was for the cosine correction. With this correction, the DNs of both corrected images, except the NIR band of the 2003 image, became more closely correlated with $i(x, y)$ with considerably increased r^2 and absolute m_λ^i values. Since the cosine correction was only intended to reduce topographic effects in the solar direction, the degree of correlation between DNs and $e(x, y)$ (i.e., m_λ^e) remained unchanged after the correction. This was also true for the *C* correction where no improvement was made in the view direction. The *C* correction in the solar direction and the Minnaert correction reduced topographic effects on the 2004 image with greatly decreased regression coefficients. However, both methods did not perform well for the 2003 image, except for the NIR band in the solar direction.

For both the visible and NIR bands, all corrections had a minimal impact on the standard deviation of DN values, indicating that none of these methods significantly changed the spatial variability of DN across the study area (Tables 3 and 4). The results were also shown in the image histogram distributions (Figs. 5 and 6). The histograms of the empirically corrected images were very close to the corresponding uncorrected images. The cosine correction tended to reduce the occurrence of medium DNs and increase the occurrence of small and large DNs, although the magnitude of changes was different for different images and bands. A similar, though

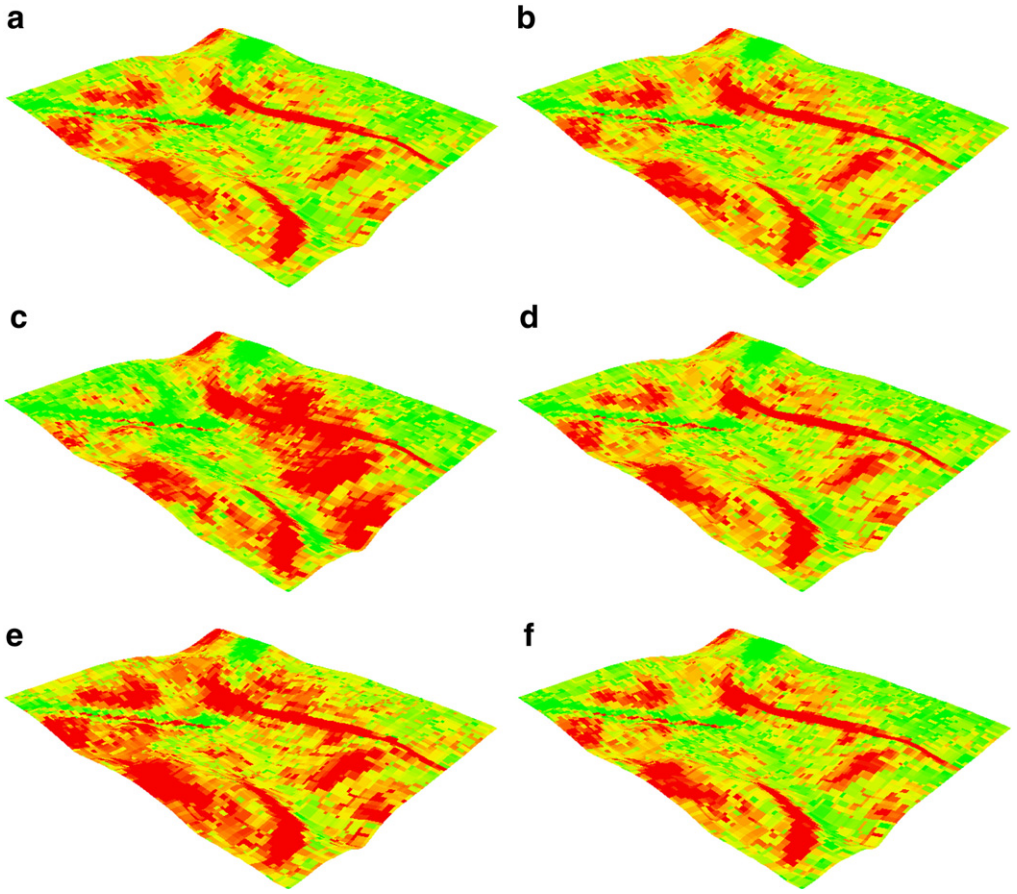

Fig. 9. Uncorrected QuickBird image in green band acquired on 20 August 2004 (a) and topographically corrected images with the empirical correction (b), the cosine correction (c), the *C* correction (d), and the Minnaert correction (e), which is also stretched to its own minimum and maximum values (f). All images are draped over the DEM.

less substantial, change was also found with the *C* correction in the visible bands of the 2003 image. The distributions of DNs with the Minnaert correction were shifted towards larger values, but remained comparable in terms of kurtosis and skewness.

3.4. Visual comparison of topographic corrections

The overall contrast of the images with the empirical and the *C* corrections (Figs. 7b, d–10b, d) did not change as impressively as those with the cosine and the Minnaert corrections (Figs. 7c, e–10c, e; for brevity, only the green band results are shown for the visible spectrum). For the images with low correlations with topography ($r^2 = 0.01$) (e.g., the blue and green bands of the 2003 image), the empirically corrected images did not change much visually, although the correction was statistically significant (Table 3). However, for the six other images with a relatively high r^2 (0.02–0.1), the empirically corrected images did show apparent changes in visual appearance, although not as evident as the cosine and the Minnaert corrections.

With the cosine correction on the 2004 image, DNs in areas having less illumination conditions (Fig. 2) significantly increased to high values (in a red or black color for the visible bands and in a green or white color for the NIR band), while DNs in areas having better illumination conditions decreased to low DN values (in a green or white color for the visible bands and in a red or black color for the NIR band) (Figs. 9c, 10c). As a result, the corrected DN values became more dependent on topography than the uncorrected values (Table 4). For the 2003 image, the cosine correction created similar, but less extensive changes in the visible bands (Fig. 7c). Because the topographic effects in the NIR band were significant and were reduced by the cosine correction as

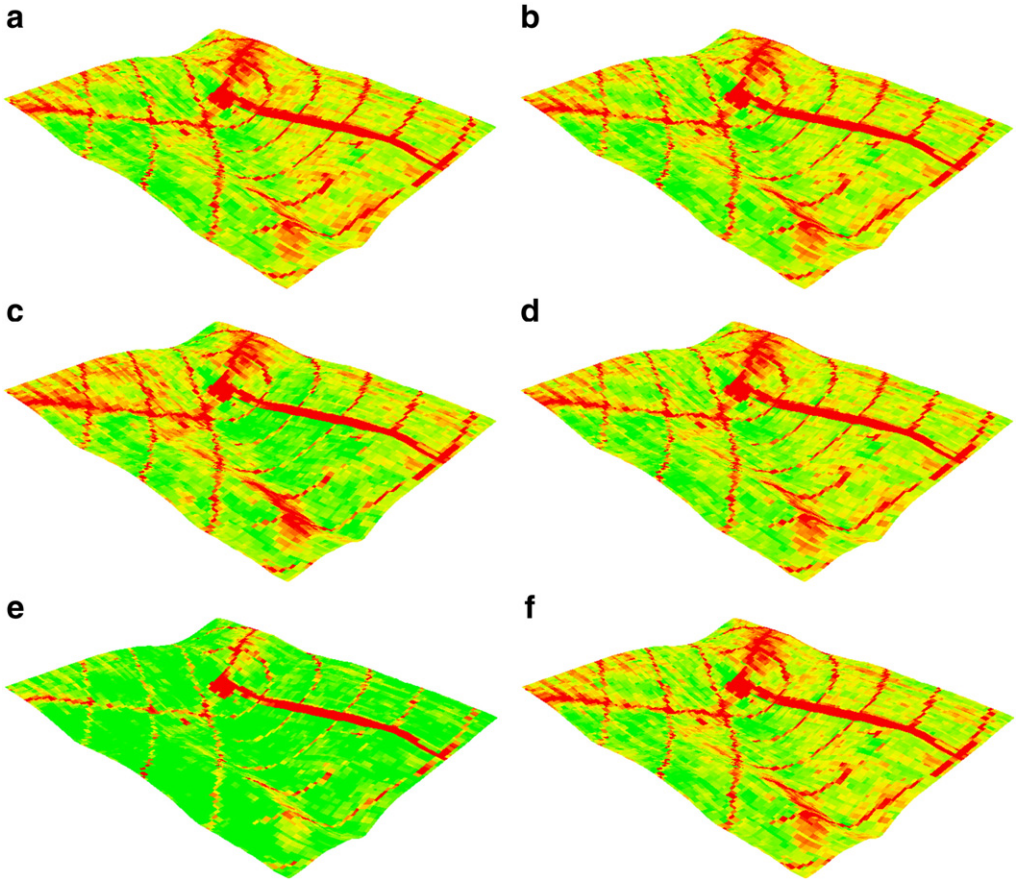

Fig. 10. Uncorrected QuickBird image in near infrared band acquired on 20 August 2004 (a) and topographically corrected images with the empirical correction (b), the cosine correction (c), the *C* correction (d), and the Minnaert correction (e), which is also stretched to its own minimum and maximum values (f). All images are draped over the DEM. Red or black circle lines are the depressed tracks traversed by the sprinkler irrigation system.

shown earlier, the visual appearance of the corrected image was close to that of the empirical and *C* corrections (Fig. 8c).

With the Minnaert correction, DNs were increased considerably to larger values, particularly for the NIR band images (with more red or black color pixels for the visible bands and more green or white color pixels for the NIR band) (Figs. 7e–10e). However, the overall spatial variability of the Minnaert corrected images did not change much, as indicated by the consistent standard deviations (Tables 3 and 4) and the minimum-maximum stretched images (Figs. 7f–10f).

4. Discussion

To generate a high resolution DEM from densely distributed high-frequency GPS measurements, it appears that the deterministic interpolation techniques based on the extent of similarity (i.e., the IDW and the polynomial methods) do not work as well as the geostatistical interpolation technique (i.e., the ordinary Kriging). Particularly, the predicted values derived from the polynomial methods had large errors since these methods are inexact interpolators that can produce estimates that go beyond the range of measurements. These errors are pronounced given that the variation of elevation in the study area is more localized and has no trend.

The variations of spectral radiances in the view direction of the 2004 image were much higher than those in the 2003 image as shown in Figs. 3 and 4 and indicated by the regression coefficients (i.e., m_λ^e) (Tables 3 and 4). The differences may be explained by the fact that the land surface on 18 July 2003 was covered with a fully-closed homogeneous crop canopy in the middle of the growing season, and that this scene was better characterized by a Lambertian reflection, while on 20 August 2004, the land

surface was covered with a partially-closed heterogeneous canopy corresponding to the late growing season, and the scene was less characterized by a Lambertian reflection.

For highly non-Lambertian surfaces, the *C* correction (in the solar direction) and the Minnaert correction appear to be able to reduce topographic effects to a certain degree. However, for land surfaces that are better characterized by a Lambertian reflection, instead of removing topographic effects, the *C* correction and the Minnaert correction may add "false" information that is not present in the uncorrected visible band images, while both methods can reduce topographic effects in NIR band images.

In an area with the relief of only a few meters, the adjustment of pixel values is a fine-tuning process compared with the substantial alteration needed in mountainous areas. Visual appearance is not always as evident as statistics in assessing a topographic correction. In addition, effective corrections do not always substantially change standard deviations and histogram distributions of imagery data.

5. Conclusions

Based on a 1 m DEM generated with high-frequency RTK GPS measurements in a moderately sloped terrain (with a maximum slope of 7.4° and a relief of 5 m), we examined the bidirectional variations of QuickBird spectral radiances with an effective solar incident angle and an emergent angle. The results showed that the spectral radiances generally varied in both solar and view directions, but the magnitude of variations depended on the optical properties of land surfaces and spectral bands. For the visible bands, a scene that was less characterized by a Lambertian reflection was more likely to be affected by the microvariation of illumination geometry than a Lambertian scene. The NIR band images were always affected by topography-induced illumination microvariations, even for a Lambertian scene.

Four topographic corrections had different degrees of effectiveness in reducing the dependence of image DN values on the illumination geometry. Among these corrections, the empirical correction proved to be the most effective method for all spectral bands in both the solar and view directions. The cosine correction gave the worst performance. The *C* correction (in the solar direction) and the Minnaert correction performed well for highly non-Lambertian surfaces, but they were less effective than the empirical correction. None of these methods significantly changed the spatial variability of the spectral radiances, but the histogram distributions were greatly modified by the cosine and Minnaert corrections and the images showed dramatic changes in their visual appearance.

Acknowledgements

QuickBird satellite images were provided by grant USDA/NASA 2001–52103–11321 and the ground measurements were supported by the grant from the University of Minnesota Graduate School Grant-In-Aid Program. We wish to acknowledge Dr. Carl Rosen and Mr. Frank Kasowski for providing the field site, and Dr. Kurt Spokas and Dr. Yi Zhang for the general assistance with GPS measurements. We also greatly appreciate the constructive suggestions of three anonymous reviewers.

References

Baral, D.J., Gupta, R.P., 1997. Integration of satellite sensor data with DEM for the study of snow cover distribution and depletion pattern. International Journal of Remote Sensing 18 (18), 3889–3894.

Barnsley, M.J., 1984. Effects of off-nadir view angles on the detected spectral response of vegetation canopies. International Journal of Remote Sensing 5 (4), 715–728.

Burrough, P.A., McDonell, R.A., 1998. Principles of Geographical Information Systems, second ed. Oxford University Press, Oxford.

Civco, D.L., 1989. Topographic normalization of Landsat Thematic Mapper digital imagery. Photogrammetric Engineering and Remote Sensing 55 (9), 1303–1309.

Cleveland, W.S., Devlin, S.J., 1988. Locally weighted regression: an approach to regression analysis by local fitting. Journal of the American Statistical Association 83 (403), 596–610.

Colby, J.D., 1991. Topographic normalization in rugged terrain. Photogrammetric Engineering and Remote Sensing 57 (5), 531–537.

Colby, J.D., Keating, P.L., 1998. Land cover classification using Landsat TM imagery in the tropical highlands: the influence of anisotropic reflectance. International Journal of Remote Sensing 19 (8), 1479–1500.

Conese, C., Gilabert, M.A., Maselli, F., Bottai, L., 1993. Topographic normalization of TM scenes through the use of an atmospheric correction method and digital terrain models. Photogrammetric Engineering and Remote Sensing 59 (12), 1745–1753.

Coops, N.C., Johnson, M., Wulder, M.A., White, J.C., 2006. Assessment of QuickBird high spatial resolution imagery to detect red attack damage due to mountain pine beetle infestation. Remote Sensing of Environment 103 (1), 67–80.

Crippen, E.R., 1988. The dangers of underestimating the importance of data adjustments in band ratioing. International Journal of Remote Sensing 9 (4), 767–776.

DigitalGlobe, Inc., 2002. QuickBird Imagery Products: Product Guide, Revision 3.3. DigitalGlobe, Colorado, Longmont.

Ekstrand, S., 1996. Landsat TM-based forest damage assessment: correction for topographic effects. Photogrammetric Engineering and Remote Sensing 62 (2), 151–161.

Giles, P.T., 2001. Remote sensing and cast shadows in mountainous terrain. Photogrammetric Engineering and Remote Sensing 67 (7), 833–839.

Holben, B.N., Justice, C.O., 1980. The topographic effect on spectral response from nadir-pointing sensors. Photogrammetric Engineering and Remote Sensing 46 (9), 1191–1200.

Huising, E.J., Gomes Pereira, L.M., 1998. Errors and accuracy estimates of laser data acquired by various laser scanning systems for topographic application. ISPRS Journal of Photogrammetry and Remote Sensing 53 (5), 245–261.

Hugli, H., Frei, W., 1983. Understanding anisotropic reflectance in mountainous terrain. Photogrammetric Engineering and Remote Sensing 49 (5), 671–683.

Itten, K.I., Meyer, P., 1993. Geometric and radiometric correction of TM data of mountainous forested areas. IEEE Transactions on Geoscience and Remote Sensing 31 (4), 764–770.

Justice, C.O., Wharton, S.W., Holben, B.N., 1981. Application of digital terrain data to quantify and reduce the topographic effect on Landsat data. International Journal of Remote Sensing 2 (3), 213–230.

Kawata, Y., Ueno, S., Kusaka, T., 1988. Radiometric correction for atmospheric and topographic effects on Landsat MSS images. International Journal of Remote Sensing 9 (4), 729–748.

Kriebel, K.T., 1978. Measured spectral bidirectional reflection properties of four vegetated surfaces. Applied Optics 17 (2), 253–259.

Meyer, P., Itten, K.I., Kellenberger, T., Sandmeier, S., Sandmeier, R., 1993. Radiometric corrections of topographically induced effects on Landsat TM data in an alpine environment. ISPRS Journal of Photogrammetry and Remote Sensing 48 (4), 17–28.

Minnaert, N., 1941. The reciprocity principle in lunar photometry. Astrophysical Journal 93 (3), 403–410.

Proy, C., Tanre, D., Deschamps, P.Y., 1989. Evaluation of topographic effects in remotely sensed data. Remote Sensing of Environment 30 (1), 21–32.

Riaño, D., Chuvieco, E., Salas, J., Aguado, I., 2003. Assessment of different topographic corrections in Landsat-TM data for mapping vegetation types. IEEE Transactions on Geoscience and Remote Sensing 41 (5), 1056–1061.

Richter, R., 1997. Correction of atmospheric and topographic effects for high spatial resolution satellite imagery. International Journal of Remote Sensing 18 (5), 1099–1111.

Sandmeier, S., Itten, K.I., 1997. A physically-based model to correct atmospheric and illumination effects in optical satellite data of rugged terrain. IEEE Transactions on Geoscience and Remote Sensing 35 (3), 708–717.

Sawaya, K.E., Olmanson, L.G., Heinert, N.J., Brezonik, P.L., Bauer, M.E., 2003. Extending satellite remote sensing to local scales: land and water resource monitoring using high-resolution imagery. Remote Sensing of Environment 88 (1–2), 144–156.

Schmidt, F., Persson, A., 2003. Comparison of DEM data capture and topographic wetness indices. Precision Agriculture 4 (2), 179–192.

Shepherd, J.D., Dymond, J.R., 2003. Correcting satellite imagery for the variance of reflectance and illumination with topography. International Journal of Remote Sensing 24 (17), 3503–3514.

Smith, J., Lin, T., Ranson, K., 1980. The Lambertian assumption and Landsat data. Photogrammetric Engineering and Remote Sensing 46 (9), 1183–1189.

Teillet, P.M., Guindon, B., Goodenough, D.G., 1982. On the slope-aspect correction of multispectral scanner data. Canadian Journal of Remote Sensing 8 (2), 84–106.

Wu, J., Wang, D., Bauer, M.E., 2005. Image-based atmospheric correction of QuickBird imagery of Minnesota cropland. Remote Sensing of Environment 99 (3), 315–325.

Wu, J., Wang, D., Rosen, C.J., Bauer, M.E., 2007a. Comparison of petiole nitrate concentrations, SPAD chlorophyll readings, and QuickBird satellite imagery in detecting nitrogen status of potato canopies. Field Crops Research 101 (1), 96–103.

Wu, J., Wang, D., Bauer, M.E., 2007b. Assessing broadband vegetation indices and QuickBird data in estimating leaf area index of corn and potato canopies. Field Crops Research 102 (1), 33–42.